Gómez-Catasús Julia (Orcid ID: 0000-0001-8949-5318)
Barrero Adrián (Orcid ID: 0000-0002-2980-1202)
Zurdo Julia (Orcid ID: 0000-0002-7283-3322)
Pérez-Granados Cristian (Orcid ID: 0000-0003-3247-4182)

Comparative assessment of satellite- and drone-based vegetation indices to predict arthropod biomass in shrub-steppes

J. Traba,[1,2,*] J. Gómez-Catasús,[1,2,3*] A. Barrero,[1,2] D. Bustillo-de la Rosa,[1,2] J. Zurdo,[1,2] I. Hervás,[1,2] C. Pérez-Granados,[1,4] E.L. García de la Morena,[1,5] A. Santamaría, [1,2] and M. Reverter[1,2]

[1] Terrestrial Ecology Group (TEG-UAM). Department of Ecology, Universidad Autónoma de Madrid. c/ Darwin, 2. 28049. Madrid, Spain

[2] Centro de Investigación en Biodiversidad y Cambio Global, Universidad Autónoma de Madrid. c/ Darwin, 2. 28049. Madrid, Spain

[3] Novia University of Applied Sciences, Raseborgsvägen 9, FI-10600 Ekenäs, Finland

[4] Ecology Department, Alicante University, PO Box 99, 03080 Alicante, Spain

[5] Biodiversity Node S.L. Sector Foresta, 17. 1º B. 28760, Tres Cantos, Madrid, Spain

[*] Equal contribution

Corresponding Author: J. Gómez-Catasús. E-mail: julia.gomez@uam.es

Open Research: All data and R-code (JGómez-Catasús, 2022) are available on Zenodo at https://doi.org/10.5281/zenodo.6621453.

This article has been accepted for publication and undergone full peer review but has not been through the copyediting, typesetting, pagination and proofreading process which may lead to differences between this version and the Version of Record. Please cite this article as doi: 10.1002/eap.2707

Abstract

Arthropod biomass is a key element in ecosystems functionality, and basic food item for many species, which must be estimated through traditional costly field sampling in normally just a few sampling points. Arthropod biomass and plant productivity should be narrowly related, as a great majority of arthropods are herbivorous, and others depends on these. Quantifying plant productivity with satellite or aerial vehicles imagery is an easy and fast procedure already tested and implemented in agriculture and field ecology. However, the ability of satellite or aerial vehicles imagery for quantifying arthropod biomass and its relationship with plant productivity has been scarcely addressed. Here, we used Unmanned Aerial Vehicle (UAV) and satellite Sentinel-2 (S2) imagery to establish relationship between plant productivity and arthropod biomass estimated through ground-truth field sampling in shrub-steppes. We UAV sampled 7 plots of 47.6-72.3 ha at 4 cm pixel resolution, and afterwards downscaling spatial resolution to 50 cm resolution. In parallel, we used S2 imagery from same and other dates and locations at 10 m spatial resolution. We related several vegetation indices (VI) with arthropod biomass (epigeous, coprophagous, and four functional consumer groups: predatory, detritivore, phytophagous and diverse) estimated in 41-48 sampling stations for UAV flying plots, and in 67-79 sampling stations for S2. VI derived from UAV were consistently and positively related with all arthropod biomass groups. Three out of seven, and six out of seven S2-derived VI were positively related with epigeous and coprophagous arthropod biomass, respectively. BNDVI and ENDVI showed consistent and positive relationships with arthropod biomass, regardless of the arthropod group and the spatial resolution. Our results point out that UAV and S2-VI imagery data may be a viable and cost-efficient alternative to quantify arthropod biomass at large scales in shrub-steppes. The relationship between VI and arthropod biomass is probably habitat-dependent and

thus, future research should address this relationship including several habitats to validate vegetation indices as proxies of arthropod biomass.

Keywords: Vegetation indices, arthropod biomass, shrub-steppe, epigeous arthropods, coprophagous arthropods

Introduction

Arthropods play a fundamental role in ecosystem functioning such as pollination, pest control, organic decomposition (Losey and Vaughan 2006), and being a key food item for many species (Báldi and Kisbenedek 1997, Weiss et al. 2013). Arthropod biomass and diversity are usually associated to plant productivity, as decreases in quantity of forage seem to reduce the amount of plant consumers (the more-individuals hypothesis; Srivastava and Lawton 1998, Kaspari et al. 2003). Moreover, plant health relates to nutrient availability, which directly may affect plant biomass and indirectly arthropod communities (Siemann 1998, Haddad et al. 2001). In summary, plant biomass and quality, as well as specific vegetation structure or composition, are related to arthropod biomass both for the whole community (Dennis et al. 1998, Harrison et al. 2018, Prather and Kaspari 2019) and for distinct taxonomic or functional groups (Báldi and Kisbenedek 1997, Weyer et al. 2012, Labadessa et al. 2015, Smith et al. 2020). Despite these considerations, establishing general relationships of arthropod biomass with specific plant characteristics may be tricky, especially at large spatial scales, due to the great diversity of the arthropod group in its size, mobility, trophic level, life history, and in their microhabitat preferences, including plant structure and composition (Southwood et al. 1979). Therefore, a more general evaluation of its relationship with plant productivity remains a challenge (but see Sweet et al. 2015, Fernández-Tizón et al. 2020).

Remote sensing has the capacity of mapping and quantifying plant productivity in different types of natural and anthropogenic influenced plant communities and land uses (Díaz-Delgado et al. 2017). Since several decades, different satellite platforms as MODIS, Landsat and other mid-spatial resolution (ten of meters) satellites have been used to explore and map plant productivity and other vegetation characteristics at large scales (e.g., Möller et al. 2017). Recently, Sentinel-2 (S2 hereinafter) has emerged as a major asset (Inglada et al. 2015, Belgiu and Csillik 2018), basically for its medium spatial (10 m), high radiometric (13 spectral bands), and rapid temporal (revisit time of 5 days at the equator) resolutions, together with its free-cost. Theoretically, it would be relatively easy to test for relationships between satellite-extracted plant productivity and other biologically relevant variables different than – but related to – plant productivity. This could be the case of animal biomass, for example, when a relation between plants and animals is predicted. However, the spatial resolution of free-satellite imagery could be too coarse to establish accurate relationships at fine scales, such as that between plant productivity and arthropod biomass. The use of Unmanned Aircraft Vehicles (UAV), which work on high- and very high- resolution imagery and allow to obtain multiple images of different dates at a relatively low-cost, may help to test these relationships. UAV has been used to provide reliable estimates of plant biomass, productivity and greenness (Colomina and Molina 2014, Strong et al. 2017, Pla et al. 2019), and even to differentiate among species (Salamí et al. 2014), but on a few occasions these relationships have been later tested at larger spatial scales, where UAV use may be inefficient (Fraser et al. 2017, Pla et al. 2019). In short, UAV combination of multispectral sensors and photogrammetric-derived information allows map productivity at very detailed scales, detect short-time changes and thus provide rapid assessment for management and conservation of other organisms, as mammals (Vermeulen et al. 2013) or breeding bird colonies (Sardà-Palomera et al. 2012). On the other side, fine and medium resolution remote sensing has

the potential to allow extrapolations to remote and non-sampled areas but, to our knowledge, it has been scarcely used to relate with other key elements in ecosystems, as arthropod biomass.

Among the remote sensing-derived products more often used are plant productivity or greenness indicators, frequently named vegetation indices (VI). VI are mathematical combination based on digital values of spectral bands, in a way designed to produce a simple value that indicates the amount or plant vigor (greenness, productivity) of vegetation within a pixel, estimated as a function of the radiation that plants emit or reflect (Rouse et al. 1974). VI can be used for detecting changes in photosynthetic activity and plant spatial heterogeneity, in order to evaluate for phenology, plant stress situations, damages or conditions, differences in soil moisture, etc., which in turn can be used to explain other ecological relationships (Huete et al. 1997, Colomina and Molina 2014, Inglada et al. 2015, Imran et al. 2020). VI are related to the proportion of radiation absorbed by photosynthetic tissues and are linearly correlated with vegetation features like the leaf area index (LAI) and plant biomass (Hunt et al. 2010, Kross et al. 2015, Prabhakara et al. 2015). Thus, VI can capture complex ecological information about canopy structure, aboveground biomass and leaf traits, or proportion of photosynthetic and non-photosynthetic parts such as leaf dry matter and bare ground (Serrano et al. 2000, Ollinger 2011).

The Normalized Difference Vegetation Index (NDVI; Rouse et al. 1974) is the VI most often used (see a review in Pettorelli et al. 2011). The majority of VI are an adaptation from NDVI and are calculated by combining two or more spectral bands. For instance, using the green band instead of the red band allows the VI to be less sensitive to variations in ground cover as vegetation has a higher level of reflectance for green wavelengths (Gitelson et al. 1996, Sripada et al. 2006). The blue channel, as in the BNDVI, amplifies the chlorophyll absorption by summing both Near-infrared (NIR) reflectance and green channel reflectance, and have been

proved useful for vegetation monitoring and a better parameterization of plant health indicators (Rasmussen et al. 2016). These other VI may operate better under determined circumstances and reduce negative effects attributed to NDVI, as those related with atmospheric conditions and soil background (Huete et al. 1997). Besides, VI using blue or green channels may perform well when trying to relate them to biological parameters (Gitelson et al. 1996, Strong et al. 2017).

Finding simple and low-cost methods to quantify arthropod abundance or biomass is a major challenge in ecology as it would provide sensitive data for many uses, including conservation, while improving the high cost–benefit ratio of field sampling. Field sampling of plant structure (plant height and cover, frequently by species) and arthropods (high number of pit-fall traps, sweep net sampling, etc.) is highly time-consuming and cost-demanding and usually provides information on just a few located points. On the contrary, UAV and satellite platforms provide affordable or even free medium to high resolution imagery, offering repeatability in time and space and can be used in remote areas (Colomina and Molina 2014, Strong et al. 2017). These characteristics make it a potential cost-efficient tool for estimating arthropod biomass. In this work we aim to test for relationships between plant biomass (estimated through different VI) and arthropod biomass (epigeous, coprophagous, and consumer groups: predatory, detritivore, phytophagous and diverse) when working at fine (UAV) and medium (S2) spatial resolution, under the hypothesis of a positive relationship between these two ecosystem components and that this relationship can be detected at both small and large spatial scales. Due to the assumed strong site-specific habitat-dependent relationships between arthropods and plant productivity (Weiss et al. 2013) and its remote sensing-derived information, we tested them in a single ecosystem, the natural Iberian shrub-steppe habitats (‘paramos’) in Central Spain. Natural steppe habitats are one of the most rare and threatened habitats in Europe (Sainz Ollero 2013). In Spain, the Iberian

'paramos' represent an important habitat of Iberian steppes (Sainz Ollero 2013) and hold singular communities of plants, arthropods and birds (Traba et al. 2013, Zurdo et al. 2021), which are intimately interrelated. Several works have detected significant relationships between plant structure, arthropod availability and threatened insectivorous bird species in these Iberian 'paramos', which point out to a complex system of multiple interactions where plant structure and composition modulates arthropod biomass and composition, which in turn influences abundance and space use of insectivorous birds (Gómez-Catasús et al. 2019, Reverter et al. 2019, Smith et al. 2020). As a consequence, some steppe bird species of high conservation interest have their strongholds in these Iberian 'paramos' (Traba et al. 2013), such as the Dupont's lark (*Chersophilus duponti*), the greater short-toed lark (*Calandrella brachydactyla*) and the tawny pipit (*Anthus campestris*), which makes even more interesting to deep in the relationship between plants and arthropods. Besides the relative homogeneous landscape and simple vegetation structure of these shrub-steppe habitats (dominated by small height scrublands and grasslands), bird distribution is not homogeneous and seems to respond to spatial heterogeneity at fine scale in plant and arthropods availability (Gómez-Catasús et al. 2019; Reverter et al. 2019, 2021), so high and medium resolution remote sensing can help us to better understand these complex ecological relationships at an appropriate scale.

Methods

Study area

The study area is located in the Iberian System (Soria, central Spain) (Fig. 1A), within the 'Altos de Barahona' and 'Páramo de Layna' Special Areas of Conservation (SAC) and Special Protection Areas (SPAs) of the European Union's Natura 2000 Network (ES4170148 and

ES4170120 respectively; Fig. 1B). They are located in the 10x10 UTM 30TWL16, 17, 26, 27, 36, 37, 46 and 55. The whole study area covers around 50400 ha in both SACs. The relief is gentle or plain (excluding river canyons, not considered in this study), located around 1100-1200 m a.s.l. Soils are shallow with rocky substrate. Climate is continental Mediterranean, with a mean temperature of 10.8ºC and a mean annual rainfall of 471 mm (Aranbarri et al. 2015).

These areas are of conservation interest due to the steppe bird community they hold, particularly the Dupont's lark, as well for including several European habitats of interest (Zurdo et al. 2021). Plant communities are dominated by continental scrublands and mixed grassland-scrublands such as *Genista pumila, G. scorpius, Thymus* spp. and *Satureja intricata,* dry perennial grasslands, and xerophytic grasslands on carbonate substrates (Sainz Ollero and van Staalduinen 2012, Zurdo et al. 2021). Crops, ploughed fields and pine afforestations are interspersed in the area, though they were explicitly excluded from the study.

Field sampling – arthropod biomass

We located a total of 92 field sampling stations to estimate arthropod biomass, but not all were placed in all sampling years: 79 in 2017, and 67 in 2018 and 2019 (Table 1). Sampling stations were separated by a mean distance of 271.7 m (SD = 170.9; minimum and maximum distances to the nearest sampling station were 117.1 m and 1781.3 m, respectively). Arthropod biomass was sampled once in winter (January/February), summer (July) and autumn (September/October), and three times during spring (April, May and June) in 2017, 2018 and 2019 (Table 1). Sampling stations were not placed in winter 2018 due to unfavorable weather conditions.

Terrestrial ground-dwelling arthropods were sampled using three pitfall traps per sampling station, placed at 5 meters intervals. Pitfall traps consisted of a plastic cup of 230 ml, 7 cm

diameter and 10 cm depth, with holes at the top to ease rain drainage. Plastic cups were buried and protected by a PVC tube to prevent its collapse and filled with 175 ml of 40% ethylene glycol and a drop of soap to reduce surface tension. Traps were active for seven days, then being filtered and animals stored in 70% ethanol. Although flying arthropods also fell into the pitfall traps, we carried out a specific sampling of flying arthropods at the moment of collecting pitfall traps in order to cover all taxa. For that, we walked two 10 m transects per sampling station with an entomological sweep net. The trapped individuals were stored in the same bottle as ground-dwelling arthropods and they were considered together, hereafter referred as epigeous arthropods. For more details about sampling methodology see Reverter et al. (2021) or Gómez-Catasús et al. (2019).

Coprophagous arthropods were sampled at each sampling station placing one baited pitfall trap, consisting of a 20 cm diameter plastic container baited with 200 g of fresh local sheep dung. Traps were active for one day, just after the collection of epigeous pitfall traps and under similar weather conditions in all sampling stations. Coprophagous arthropods were stored in 70% ethanol and only those individuals with coprophagous habits were identified: order *Coleoptera* family *Scarabaeidae* (*Gymnopleurus* spp., *Onthophagus* spp. and *Scarabeus* spp.) and order *Diptera* suborder *Brachycera*.

We determined arthropods at least to its taxonomic order. We estimated arthropod biomass using the specific equations from Hódar (1996):

$$W = \alpha \cdot BLb$$

where W is biomass in mg, BL is body length (in mm) and α and b are specific parameters for each group (or each order) (Hódar 1996). We measured body length (excluding legs, antennas

and other appendices) in a maximum of 15 individuals per sample, using a digital calliper (± 0.01 mm). To minimize observer bias, all samples were identified by the same researcher (MR). For a similar methodology for estimation of invertebrate biomass see Traba et al. (2007), Gómez-Catasús et al. (2019) or Reverter et al. (2021). Lastly, we classified epigeous arthropod taxa into consumer groups (predatory, detritivore, phytophagous and diverse; Appendix S1) and calculated the biomass per each arthropod consumer group.

Since three pitfall traps were placed per sampling station, the biomass of epigeous arthropods (terrestrial + flying) per station and sampling period was estimated as the mean biomass of the pitfall traps that were active after seven days. Lastly, coprophagous arthropod biomass was estimated as the total biomass measured in each sampling station, since only one baited pitfall trap was placed per sampling station. In case the trap was invalidated, it was noted as missing data.

UAV imagery collection

We selected seven plots (Fig. 1B) ranging from 47.6 to 72.3 ha (mean ± SD = 60.0 ± 9.6) within the general study area (Fig. 1B). Plots were similar in relation with altitude, relief, slope and plant communities. A total of 41 sampling stations were placed within six plots in 2017, and 48 sampling stations within seven plots in 2018 out of the above mentioned 92 sampling stations (Table 1).

During five time points along the years 2017 and 2018 we carried out up to 65 flights, with near 28 flight hours and 1290 km travelled, with a total of 20881 images obtained. A summary on flights can be found in Appendix S2. Specific flight dates were always close to the field sampling addressed to estimate arthropod biomass (see above; Table 1).

UAV high-resolution images were collected using a fixed-wing drone (SRPAS model A2) flying 120 m above the ground (equivalent to a focal length of 5.2 mm), which offered a resolution on the ground (GSD) of 4 cm/pixel. In general, each of the seven study plots was completely covered in a single flight, although some minor sections or even the entire sector was repeated in case of technical or meteorological incidents.

The sensor was a Canon S100 camera modified to capture the red edge spectrum (approx. 770 nm; filter Event38), with a 1/1.7" CMOS sensor and 12 MP resolution. This modified sensor provides images along three discrete spectral bands: Red Edge (RE), Green and Blue. Despite the relatively low-accuracy band-discrimination capacity of this type of modified cameras compared to that of traditional multispectral cameras, they offer good solutions with a high cost-benefit relationship for estimating productivity indices in the field of agriculture or field ecology (Lebourgeois et al. 2008, Salamí et al. 2014). RE channel was around 770 nm, which may correspond to a mid-position between channels 6 and 7 in S2. Images post-processing consisted in: i) georeferencing (in the WGS84 system) and altitude registering; ii) image aligning and building of the digital elevation model (DEM) and the orthomosaic, using the Agisoft Metashape Professional photogrammetry software (Version 1.4). Georeferencing was carried out with 4-6 permanent ground control points per study plot, determined with submeter precision using a GNSS system with differential correction in real time, Emlid Reach. Finally, iii) we downscaled the resolution of the orthophotos to a 50 cm/pixel while calculating the different VI, in order to reduce the size of the files and facilitate data processing but maintaining a high spatial resolution.

Sentinel-2 imagery collection

We used free S2 imagery atmospherically-corrected, corresponding to the 30TVL and 30TWL zones, where all the 92 field sampling points were located (see below). We selected available

cloud-free images corresponding to the closest date to each arthropod field sampling (Table 1), always in the same date for both UTM zones. Imagery was obtained from "LandViewer" page (eos.com). We used Blue, Green, Red and NIR (channel 8) bands to calculate VI, with a spatial resolution of 10 m.

Vegetation indices (VI)

We calculated the following VI: BNDVI, ENDVI, GIPVI, GNDVI, GRVI, GSAVI, for UAV imagery, and the same indices and NDVI for S2 imagery (see Table 2). All these indices were obtained by applying the corresponding formula (Table 2) on the digital numbers coming from the corresponding channels of the UAV or S2 imagery and saved in a raster layer with TIF extension. VI from UAV imagery were calculated using the RE band instead of the NIR band, because the modified sensor employed did not provide images along the NIR spectral band (see *UAV imagery collection*). Previous studies have demonstrated that VI calculated using RE and visible bands show similar performance in estimating variables associated to plant productivity, vigor, or health than those using NIR (Upadhyay et al. 2013, Imran et al. 2020). In our case, S2-derived VI calculated using both RE and NIR bands were highly correlated, leading to similar results (see Appendix S3).

We calculated VI assigned to each arthropod sampling station as the average of each index in a 50 m buffer around the central point of each sampling station, for both UAV and S2 imagery. VI calculations, zone statistics and spatial joining were carried out in an open GIS (Quantum GIS Development Team 2020).

Statistical analysis

Response variables (epigeous and coprophagous arthropod biomass, as well as biomass of predatory, detritivore, phytophagous and diverse groups) were log-transformed to achieve linearity, and fixed covariates were z-standardized (mean=0 and SD=1). Explanatory variables (season, year, and each vegetation index independently) were tested for collinearity prior to data analysis, and all predictors were retained as all had a generalized variance inflation factor (GVIF) lower than 2 (Fox and Monette 1992).

We explored fine-scale (UAV) and coarse-scale (S2) relationships between the different groups of arthropod biomass (epigeous and coprophagous, on the one hand, and predatory, detritivore, phytophagous and diverse on the other), and each of the VI calculated from UAV and S2 imagery, respectively. For this purpose, we fitted a separate linear regression model (Gaussian error distribution) for each arthropod group (response variable) and each vegetation index (covariate), so that the relationship was evaluated independently for each arthropod group and for each vegetation index. In addition, we incorporated a spatial dependency component to account for potential non-independence of data collected from nearby sampling stations. This was carried out by incorporating a spatial random effect (i.e., random factor) using Integrated Nested Laplace Approximation with Stochastic Partial Differential Equations (INLA-SPDE; Lindgren et al. 2011). Spatial dependency of observations is accounted for using a latent Gaussian random field, which we constructed using two-dimensional irregular grids (meshes) based on the geographic coordinates of the sampling stations. The mesh divides the study area in a large number of non-overlapping triangles (i.e., Delaunay triangularization), and it will be employed to approximate the solution of the SPDE that defines the spatial process with a Matérn covariance (Zuur et al. 2017; Gómez-Rubio, 2020). Specifically, we constructed two meshes using the sampling stations at S2 and UAV limits, respectively. Meshes were built using a non-convex boundary for the

coordinates of sampling stations, and with a buffer zone in order to avoid edge effects for the bordering vertices (Zuur et al. 2017) (see Appendix S4). An independent model was fitted for each VI, incorporating both linear and quadratic forms of the VI as predictors to control for non-linear relationships. Orthogonal polynomials were obtained using the function poly from the R-package stats (R Core Team 2020), avoiding high GVIF values and potential collinearity among predictors. Moreover, we incorporated the factors year (2017/2018 for UAV and 2017/2018/2019 for S2) and season (Spring/Summer/Autumn for UAV and Winter/Spring/Summer/Autumn for S2) as predictors in order to control for potential inter- and intra-annual variability on epigeous and coprophagous biomass, although no evaluation or discussion of these results are presented (see Appendix S5 for these results).

The VI calculated from UAV and S2 imagery are expected to have a spatial pattern and thus, spatial confounding might be a potential problem in our analyses. Spatial confounding occurs when the covariates are collinear with the spatial random effects, leading to bias and variance inflation of the fixed effects and hence erroneous inference (Hodges and Reich 2010, Hanks et al. 2015). To overcome this problem, one potential solution is to constrain the spatial random to be orthogonal to those fixed effects with a spatial pattern (Hodges and Reich 2010, Adin et al. 2020). We tested for spatial confounding in our models by fitting linear regression models incorporating the spatial random intercepts for each observation (response variable) and the VI as predictors (Hanks et al. 2015). We considered the existence of spatial confounding when the 95% Bayesian Credible Interval (95% BCI) for the VI under consideration did not contain 0, which means that the spatial random intercepts and the VI involved are correlated (see Appendix S6 for results on spatial confounding assessment). In the presence of spatial confounding, we fitted

spatial linear regression models (Gaussian error distribution) constraining the spatial random effect to be orthogonal to the VI (extraconstr argument in INLA; Gómez-Rubio 2020).

All models were fitted using the R package INLA (Rue et al. 2009) in the free R software (v.4.0.3; R Core Team 2020). We used INLA default prior distributions for the intercept $\alpha \sim N(0,0)$, and the regression coefficients $\beta \sim N(0, 1000)$ (Gómez-Rubio 2020). Parameter estimates were reported as the posterior mean (β), associated standard deviation (SD) and the 95% Bayesian Credible Interval (95% BCI). We considered predictors to have an effect on the response variable when the parameter's 95% BCI did not overlap zero (Zuur et al. 2017).

Results

VI calculated from UAV imagery showed higher correlation values (mean ± SD of the Pearson correlation coefficients = 0.92 ± 0.09) than those calculated from S2 imagery (0.88 ± 0.13; see Appendix S7). Moreover, VI from UAV imagery showed low correlation values with those VI from S2 imagery (0.47 ± 0.09; see Appendix S7). Overall, VI calculated from S2 had higher values than those from UAV imagery (Table 3). All vegetation indices calculated from UAV imagery had higher values in spring than autumn. All S2-derived indices showed their highest values in winter (except for NDVI, which was equal in winter and spring). BNDVI and ENDVI reached their lowest value in summer, GIPVI, GNDVI, GRVI and GSAVI in summer and autumn, and NDVI in autumn (see Appendix S8 for a more detailed description of the inter- and intra-annual variability in the VI).

The biomass of arthropods also varied along the year (Table 4). During the winter we recorded the lowest biomass values per sampling station for all groups, increasing considerably during the spring. In the summer we observed less consistent responses, including negative (predatory and

detritivore arthropods), stable (epigeous and diverse arthropods), and positive trends (coprophagous and phytophagous arthropods; Table 4). Most arthropod groups decreased during the autumn except for predatory and phytophagous arthropods that experienced an increase, being the highest values recorded throughout the year for the phytophagous arthropods (Table 4).

Relationship between arthropod biomass and Vegetation Indices from UAV imagery

All VI from UAV imagery showed a positive relationship with the biomass of epigeous and coprophagous arthropods. The ENDVI index was positively related with the biomass of epigeous arthropods until a threshold from which the increase slowed down (quadratic term in Table 5; Fig. 2). The remaining VI showed a positive linear relationship with the epigeous biomass (Table 5; Fig. 2). All consumer groups showed a positive relationship with all VI, except for detritivore arthropods that did not show any relationship with ENDVI index and for diverse arthropods which did not show any relationship with GRVI index (see Appendix S9 for arthropod group results). Lastly, all VI calculated from UAV imagery showed a positive linear relationship with the biomass of coprophagous arthropods (Table 5; Fig. 3).

Relationship between arthropod biomass and Vegetation Indices from Sentinel-2 imagery

In the case of the VI calculated from the S2 imagery, not all VI showed a relationship with the biomass of epigeous and coprophagous arthropods. The NDVI index calculated from S2 imagery showed a negative relationship with the biomass of epigeous arthropods (Fig. 4). The BNDVI and the ENDVI indices were positively related with epigeous biomass (both linear and quadratic terms; Table 6; Fig. 4), whereas the remaining indices did not show any relationship with epigeous biomass (Table 6). Regarding the biomass of each consumer group we observed that ENDVI and BNDVI indices were positively related with the biomass of predatory, detritivore

and diverse arthropods, but not for the biomass of phytophagous arthropods. Moreover, the NDVI index was negatively related with the biomass of phytophagous arthropods, but not with the other consumer groups. All other vegetation indices were only positively related with the biomass of predatory arthropods (see Appendix S9 for these results). Lastly, all VI were positively related with coprophagous biomass, except for the NDVI index that did not show any relationship (Table 6; Fig. 5).

Discussion

Information about ecological patterns and processes at large spatial scales is essential for both basic and applied studies. However, the effort required to field-collect this type of data may be unaffordable, especially for some specific organisms, and its applicability at large spatial scales can be then restricted. Thus, the use of remote sensing imagery to search and map natural processes at large or very large spatial scales offers great possibilities. This work has shown a solid positive relationship between different remote sensing-derived VI and arthropod biomass, even after accounting for seasonal and interannual variability and geographic position. This relationship was especially strong and consistent when working with fine-scale UAV-derived VI, but it was also found with several coarser-scale S2-derived VI, which consequently provides a strong capacity to use raster imagery in order to extrapolate information on unexplored or non-sampled areas.

Despite the difference in channels used for estimating VI between UAV and S2 imagery, our results seem conclusive about the relationship between VI and arthropod biomass. Indeed, both VI calculated from the NIR and the RE bands in our sampling stations located in shrub-steppes were highly correlated, and consequently, modelling results using RE were basically the same than those using NIR and exposed in the Results section (see Appendix S3). Thus, we consider

that our results are solid regardless the channel used. Our results are concordant with several previous works carried out on different habitat types that found a strong correlation between S2 RE and NIR derived VI, though the firsts were even less affected by plants traits, especially when assessing temporal variation (Upadhyay et al. 2013, Sweet et al. 2015, Fernández-Tizón et al. 2020, Imran et al. 2020).

Our results showed strong relationship between all UAV-derived VI and epigeous arthropod biomass (see also results on consumer functional groups in Appendix S9). In the case of S2-derived VI, however, only two VI (BNDVI and ENDVI) showed a positive relationship with the biomass of epigeous arthropods, whereas one VI (NDVI) showed a negative relationship which could be primarily driven by the negative relationship observed between phytophagous arthropods and S2-derived NDVI (Appendix S9). These differences between VI might be explained by the observed discrepancies in the intra-annual variation of the S2-derived VI, with autumn being the season in which these discrepancies were most evident (Appendix S8). S2-derived BNDVI and ENDVI increased in autumn, whereas GIPVI, GNDVI, GRVI and GSAVI remained stable and NDVI decreased compared to the summer values (Appendix S8). Our results suggest that BNDVI and ENDVI might give better estimations of plant productivity in autumn in shrub-steppes and thus, of arthropod biomass throughout the year. However, future research should address the relationship between field measurements of plant productivity and VI values to better understand the discrepancies observed between S2-derived VI, and to elucidate which index is the best indicator of plant productivity in shrub-steppes and thus, of arthropod biomass.

The highest performance of UAV versus S2-derived vegetation indices to relate with arthropod biomass may be explained by differences in spatial resolution. UAV-derived VI were calculated at 50 cm resolution (after downscaling from initial 4 cm resolution), while S2-derived VI were at

10 m resolution. The same reasoning might be also valid to explain differences among the VI values estimated using UAV and S-2, since the values of the same index greatly differ with the approach employed. In the case of epigeous arthropod biomass, a small-spatial scale relationship with vegetation could be expected (Báldi and Kisbenedek 1997, Weyer et al. 2012, Labadessa et al. 2015), as epigeous arthropods include species both sedentary and of some mobility (Dennis et al. 1998). Thus, the relationship may be more difficult to be found when spatial resolution is coarser (see however; Fernández-Tizón et al. 2020). Changes in spatial resolution, as mentioned above, can modify the determination coefficient of greenness indices, and thus, changing the greenness values of each pixel (Prabhakara et al. 2015, Díaz-Delgado et al. 2017). Another complementary explanation may help to understand differences between UAV and S2 results. Chlorophyll absorption range is usually between 400–700 nm (Ollinger 2011), while in our case UAV-derived VI used the RE channel, which is above 700 nm. Besides, S2-derived VI estimated with the Red-edge channel showed similar results (Appendix S3), which suggests that changes should be linked to spatial resolution more than to radiometric effects. In any case, more research is needed in this sense in order to disentangle which radiometrically detected elements are related to arthropod activity and biomass.

We found a strong and consistent positive relationship between epigeous arthropod biomass and vegetation, except for S2-derived NDVI. Arthropods seem to be an especially suitable group to be related with plant productivity as their response to changes in plant community are faster than those of vertebrates (Thomas et al. 2004). Previous works have also found strong, although not always linear relationships between arthropod abundance or biomass and plants traits related with productivity such size, plant condition or leaf area (see for instance Sweet et al. 2015, Harrison et al. 2018, Prather and Kaspari 2019, Fernández-Tizón et al. 2020, Smith et al. 2020). In summary,

increases in plant productivity promotes higher abundance of arthropod herbivores (Carmona et al. 2011, Smith et al. 2020), which in turn increases arthropod predator and parasite populations (Langellotto and Denno 2004, Prather and Kaspari 2019, Smith et al. 2020). In our case, predatory arthropods showed a positive linear relationship with all VI (except for the NDVI index), whereas detritivore and diverse arthropods showed positive relationships with BNDVI and ENDVI S2-derived indices. However, phytophagous arthropods showed a negative relationship with S2-derived NDVI (Appendix S9). In the case of S2-derived NDVI, our results are counterintuitive, as we expected a similar positive relationship than that found in the rest of VI. This may be because phytophagous arthropod biomass reaches its maximum values in autumn and minimum values in winter (Table 4), when the NDVI reaches its minimum and maximum values, respectively (Appendix S8). In any case, in shrub steppe habitats where bare ground cover is especially high and shrubs with pointed and thin leaves predominate (Zurdo et al. 2021), NDVI seems to show inverse behavior than green channel-based VI, perhaps due to its higher level of reflectance for green wavelengths (Gitelson et al. 1996, Sripada et al. 2006). In a previous work, Sweet et al. (2015) showed that estimates of NDVI calculated at 1 m^2 quadrats by field portable spectroradiometer correlated positively with arthropod biomass. Fernández-Tizón et al. (2020) found positive significant relationship between satellite-derived NDVI and arthropod biomass in semi-natural grasslands in central Europe, though the spatial resolution of satellite imagery was extremely coarser than ours (16x16 km), and thus it had a lower extrapolation capacity. None of these mentioned works, as well as our own work, showed relationships with a maximum between VI and biomass, suggesting that maximums are probably out of the studied indices (habitats). Despite the remarkable utility of satellite-derived VI (and specially NDVI) in animal ecology (Pettorelli et al. 2011), our results suggest the need of more study in differences between VI and their relationships with biodiversity elements.

In the case of coprophagous arthropods, all UAV- and near all S2-derived VI except for NDVI, showed a positive relationship with the biomass of coprophagous arthropods. In this case, coprophagous group includes high-mobility species that are attracted to a baited trap, sometimes from long distances (Dormont et al. 2007, Perrin et al. 2019) and independently from the characteristics of the aboveground vegetation where the trap is located. Our results, being so solid both for UAV and S2 suggest that the coprophagous species pool attracted to a baited trap might be highly local and dependent on other exogenous factors as the abundance of dung of herbivorous mammals. Extensive sheep grazing, as well as the abundance of wild herbivorous, is probably more intense where plant productivity is higher. Then, in a circular way, plant productivity is expected to be higher in sites where dung-processing arthropods are more abundant, as their activity increases nutrient content in the soil (Prather and Kaspari 2019).

A remarkable result of this work is the high similarity among VI in their relationship with arthropod biomass. In the case of UAV-derived VI, all indices showed a linear relationship with both epigeous and coprophagous arthropod biomass. In the case of S-2-derived VI, the relationship was not so obvious nor lineal for epigeous, but much more evident and lineal for the case of coprophagous. Since the proposition of the first VI, including NDVI (Rouse et al. 1974), a very high number of remote sensing-derived indices exploring plant productivity, biomass, health and/or vigor have been proposed. Many of them rely on the relation between NIR or RE and the visual range of the spectrum, posing the differences in the distinctive absorbance spectrum of chlorophyll between red (or blue, or green) and near-infrared (or red edge) regions. As in other cases (see, for instance Viña et al. 2011), our comparison between VI yielded inconclusive results in order to select the best index, but on the contrary suggest that near all the indices performed satisfactorily to predict arthropod biomass, except for NDVI despite being the

most commonly used index. In any case, our results are most probably habitat-dependent (Weiss et al. 2013), and extrapolations for different habitats/regions should include previous ground-truth field work. Iberian steppe habitats are not especially productive, as they are subjected to a high thermal range, with extremely low winter temperatures and high temperatures during summer, low annual precipitation, and frequently in the form of snow (Aranbarri et al. 2015). Under these circumstances, positive relationships between arthropod biomass and vegetation indices may be expected.

Conclusion

Our results show that remote sensing imagery and VI derived may performed satisfactorily as proxies of arthropod biomass in shrub-steppes. We found slight differences between VI in their general performance of explaining arthropod biomass. If considering the potential of close site-dependence of our results, the selection of optimal VI would depend on previous calibration between remote and field data. Anyway, our results showed that all the UAV-derived VI evaluated performed satisfactory for estimating arthropod biomass. For the case of S-2 derived VI, only BNDVI and ENDVI performed well in the case of epigeous biomass, and all but NDVI in the case of coprophagous. Thus, in the case of a particular index having to be chosen, we suggest using BNDVI or ENDVI, as they were the only two indices showing strong and consistent relations for all the arthropod groups and spatial resolutions tested. Though low-cost UAV are in constant development, total expenses derived from using UAV are difficult to be estimated and frequently are finally not so low (Jiménez López and Mulero-Pázmány 2019), especially if the study area is large. In those cases, we recommend using Sentinel free imagery and BNDVI or ENDVI as a proxy of arthropod biomass in shrub-steppes, after being adequately calibrated the relationship, especially in remote or unsampled areas. Arthropod biomass seems to

be positively related to plant biomass and vigor, which in turn, may be benefited by natural fertilization from extensive grazing. Thus, maintenance of extensive sheep grazing should result in increased arthropod biomass and diversity, and consequently in healthier populations of insectivorous birds.

Acknowledgments

Many people have collaborated during all these years in field-collecting and lab-processing samples. We wish to thank to Inmaculada Abril-Colón, Ana Santos, Filipo Colla, Álvaro Ortega, Miguel Muñoz, and Adaia Cid. We also thank Juan Corley and two anonymous revieweres whose comments helped to improve the manuscript. This study was partially supported by the European Commission (Life Ricotí project LIFE15-NAT-ES-000802 and Life Connect Ricotí project LIFE20-NAT-ES-000133) and the BBVA Foundation (BBVA-Dron Ricotí project). This paper contributes to project REMEDINAL-3 from CAM.

Conflict of interest statement

The authors declare no conflict of interest

Author contribution

JT and EGM conceived the original idea, and JT supervised the project. JT and IH secure funding. JG-C curated and analyzed data. AB, DB-R, MR and JG-C prepared original data bases. AB and EGM calculated the Vegetation Indices from UAV imagery, DB-R calculated the Vegetation Indices from Sentinel-2 imagery, and MR and JZ carried out lab work. JG-C, AB, DB-R, JZ, CPG, AS and MR carried out field work. EGM did drone flights and prepared raster

data. JT and JG-C took the lead in writing the manuscript, and all authors provided critical feedback and contributed to the final manuscript.

References

Adin, A., T. Goicoa, J. S. Hodges, P. Schnell, and M. D. Ugarte. 2020. Alleviating confounding in spatio-temporal areal models with an application on crimes against women in India. arXiv:2003.01946.

Aranbarri, J., P. González-Sampériz, E. Iriarte, A. Moreno, M. Rojo-Guerra, L. Peña-Chocarro, B. Valero-Garcés, M. Leunda, E. García-Prieto, M. Sevilla-Callejo, G. Gil-Romera, D. Magri, and J. Rodríguez-Lázaro. 2015. Human-landscape interactions in the Conquezuela-Ambrona Valley (Soria, continental Iberia): From the early neolithic land use to the origin of the current oak woodland. Palaeogeography, Palaeoclimatology, Palaeoecology 436:41–57.

Báldi, A., and T. Kisbenedek. 1997. Orthopteran assemblages as indicators of grassland naturalness in Hungary. Agriculture, Ecosystems and Environment 66:121–129.

Belgiu, M., and O. Csillik. 2018. Sentinel-2 cropland mapping using pixel-based and object-based time-weighted dynamic time warping analysis. Remote Sensing of Environment 204:509–523.

Carmona, D., M. J. Lajeunesse, and M. T. J. Johnson. 2011. Plant traits that predict resistance to herbivores. Functional Ecology 25:358–367.

Colomina, I., and P. Molina. 2014. Unmanned aerial systems for photogrammetry and remote sensing: A review. ISPRS Journal of Photogrammetry and Remote Sensing 92:79–97.

Dennis, P., M. R. Young, and I. J. Gordon. 1998. Distribution and abundance of small insects and arachnids in relation to structural heterogeneity of grazed, indigenous grasslands. Ecological

Entomology 23:253–264.

Díaz-Delgado, R., C. Hurford, and R. Lucas. 2017. Introducing the Book "The Roles of Remote Sensing in Nature Conservation." Pages 3–10 The Roles of Remote Sensing in Nature Conservation. Springer, Cham, Switzerland.

Dormont, L., S. Rapior, D. B. McKey, and J. P. Lumaret. 2007. Influence of dung volatiles on the process of resource selection by coprophagous beetles. Chemoecology 17:23–30.

Fernández-Tizón, M., T. Emmenegger, J. Perner, and S. Hahn. 2020. Arthropod biomass increase in spring correlates with NDVI in grassland habitat. Science of Nature 107:1–7.

Fox, J., and G. Monette. 1992. Generalized collinearity diagnostics. Journal of the American Statistical Association 87:178–183.

Fraser, R. H., J. van der Sluijs, and R. J. Hall. 2017. Calibrating satellite-based indices of burn severity from UAV-derived metrics of a burned boreal forest in NWT, Canada. Remote Sensing 9:279.

Gitelson, A. A., Y. J. Kaufman, and M. N. Merzlyak. 1996. Use of a green channel in remote sensing of global vegetation from EOS- MODIS. Remote Sensing of Environment 58:289–298.

Gómez-Catasús, J., V. Garza, M. B. Morales, and J. Traba. 2019. Hierarchical habitat-use by an endangered steppe bird in fragmented landscapes is associated with large connected patches and high food availability. Scientific Reports 9:1–12.

Gómez-Rubio, V. 2020. Bayesian inference with INLA. Chapman & Hall/CRC Press, Boca Raton, Florida.

Haddad, N. M., D. Tilman, J. Haarstad, M. Ritchie, and J. M. H. Knops. 2001. Contrasting effects of plant richness and composition on insect communities: A field experiment. American

Naturalist 158:17–35.

Hanks, E. M., E. M. Schliep, M. B. Hooten, and J. A. Hoeting. 2015. Restricted spatial regression in practice: Geostatistical models, confounding, and robustness under model misspecification. Environmetrics 26:243–254.

Harrison, J. G., C. S. Philbin, Z. Gompert, G. W. Forister, L. Hernandez-Espinoza, B. W. Sullivan, I. S. Wallace, L. Beltran, C. D. Dodson, J. S. Francis, A. Schlageter, O. Shelef, S. A. Yoon, and M. L. Forister. 2018. Deconstruction of a plant-arthropod community reveals influential plant traits with nonlinear effects on arthropod assemblages. Functional Ecology 32:1317–1328.

Hódar, J. A. 1996. The use of regression equations for estimation of arthropod biomass in ecological studies. Acta Oecologica 17:421–433.

Hodges, J. S., and B. J. Reich. 2010. Adding spatially-correlated errors can mess up the fixed effect you love. American Statistician 64:325–334.

Huete, A. R., H. Q. Liu, K. Batchily, and W. Van Leeuwen. 1997. A comparison of vegetation indices over a global set of TM images for EOS-MODIS. Remote Sensing of Environment 59:440–451.

Hunt, E. R., W. Dean Hively, S. J. Fujikawa, D. S. Linden, C. S. T. Daughtry, and G. W. McCarty. 2010. Acquisition of NIR-green-blue digital photographs from unmanned aircraft for crop monitoring. Remote Sensing 2:290–305.

Imran, H. A., D. Gianelle, D. Rocchini, M. Dalponte, M. P. Martín, K. Sakowska, G. Wohlfahrt, and L. Vescovo. 2020. VIS-NIR, red-edge and NIR-shoulder based normalized vegetation indices response to co-varying leaf and Canopy structural traits in heterogeneous grasslands. Remote Sensing 12:2254.

Inglada, J., M. Arias, B. Tardy, O. Hagolle, S. Valero, D. Morin, G. Dedieu, G. Sepulcre, S. Bontemps, P. Defourny, and B. Koetz. 2015. Assessment of an operational system for crop type map production using high temporal and spatial resolution satellite optical imagery. Remote Sensing 7:12356–12379.

JGomez-Catasus. 2022. JGomez-Catasus/Primary-productivity-correlates-with-arthropod-biomass-comparing-satellite--and-drone-based-vegetat: Comparative assessment of satellite- and drone-based vegetation indices to predict arthropod biomass in shrub-steppes (v.1.0.0). Zenodo. https://doi.org/10.5281/zenodo.6621453

Jiménez López, J., and M. Mulero-Pázmány. 2019. Drones for conservation in protected areas: Present and future. Drones 3:10.

Kaspari, M., M. Yuan, and L. Alonso. 2003. Spatial grain and the causes of regional diversity gradients in ants. American Naturalist 161:459–477.

Kross, A., H. McNairn, D. Lapen, M. Sunohara, and C. Champagne. 2015. Assessment of RapidEye vegetation indices for estimation of leaf area index and biomass in corn and soybean crops. International Journal of Applied Earth Observation and Geoinformation 34:235–248.

Labadessa, R., L. Forte, and P. Mairota. 2015. Exploring Life Forms for Linking Orthopteran Assemblage and Grassland Plant Community. Hacquetia 14:33–42.

Langellotto, G. A., and R. F. Denno. 2004. Responses of invertebrate natural enemies to complex-structured habitats: A meta-analytical synthesis. Oecologia 139:1–10.

Lebourgeois, V., A. Bégué, S. Labbé, B. Mallavan, L. Prévot, and B. Roux. 2008. Can commercial digital cameras be used as multispectral sensors? A crop monitoring test. Sensors 8:7300–7322.

Lindgren, F., H. Rue, and J. Lindström. 2011. An explicit link between gaussian fields and gaussian markov random fields: The stochastic partial differential equation approach. Journal of the Royal Statistical Society. Series B: Statistical Methodology 73:423–498.

Losey, J. E., and M. Vaughan. 2006. The economic value of ecological services provided by insects. BioScience 56:311–323.

Möller, M., H. Gerstmann, F. Gao, T. C. Dahms, and M. Förster. 2017. Coupling of phenological information and simulated vegetation index time series: Limitations and potentials for the assessment and monitoring of soil erosion risk. Catena 150:192–205.

Ollinger, S. V. 2011. Sources of variability in canopy reflectance and the convergent properties of plants. New Phytologist 189:375–394.

Perrin, W., P. Jay-Robert, B. Buatois, and L. Tatin. 2019. A Comparative Analysis of Dung Beetle Assemblages (Coleoptera: Scarabaeidae: Scarabaeinae, Aphodiinae) Attracted to Sheep and Little Bustard Excrement in Southern France. The Coleopterists Bulletin 73:185–192.

Pettorelli, N., S. Ryan, T. Mueller, N. Bunnefeld, B. Jedrzejewska, M. Lima, and K. Kausrud. 2011. The Normalized Difference Vegetation Index (NDVI): Unforeseen successes in animal ecology. Climate Research 46:15–27.

Pla, M., G. Bota, A. Duane, J. Balagué, A. Curcó, R. Gutiérrez, and L. Brotons. 2019. Calibrating sentinel-2 imagery with multispectral UAV derived information to quantify damages in mediterranean rice crops caused by western swamphen (Porphyrio porphyrio). Drones 3:45.

Prabhakara, K., W. Dean Hively, and G. W. McCarty. 2015. Evaluating the relationship between biomass, percent groundcover and remote sensing indices across six winter cover crop fields in Maryland, United States. International Journal of Applied Earth Observation and

Geoinformation 39:88–102.

Prather, R. M., and M. Kaspari. 2019. Plants regulate grassland arthropod communities through biomass, quality, and habitat heterogeneity. Ecosphere 10:e02909.

Quantum GIS Development Team. 2020. Quantum GIS Geographic Information System. Open Source Geospatial Foundation Project. http://qgis.osgeo.org.

R Core Team. 2020. R: A language and environment for statistical computing.Vienna, Austria: R Foundation for Statistical Computing. http://www.r-project.org.

Rasmussen, J., G. Ntakos, J. Nielsen, J. Svensgaard, R. N. Poulsen, and S. Christensen. 2016. Are vegetation indices derived from consumer-grade cameras mounted on UAVs sufficiently reliable for assessing experimental plots? European Journal of Agronomy 74:75–92.

Reverter, M., J. Gómez-Catasús, A. Barrero, C. Pérez-Granados, D. Bustillo-de La Rosa, and J. Traba. 2019. Interactions in shrubsteppes: Implications for the maintenance of a threatened bird. Ecosistemas 28:69–77.

Reverter, M., J. Gómez-Catasús, A. Barrero, and J. Traba. 2021. Crops modify habitat quality beyond their limits. Agriculture, Ecosystems & Environment 319: 107542.

Rouse, J. W., R. H. Haas, J. A. Schell, and D. W. Deering. 1974. Monitoring vegetation systems in the Great Plains with ERTS. NASA special publication 351:309–317.

Rue, H., S. Martino, and N. Chopin. 2009. Approximate Bayesian inference for latent Gaussian models by using integrated nested Laplace approximations. Journal of the Royal Statistical Society. Series B: Statistical Methodology 71:319–392.

Sainz Ollero, H. 2013. Steppes across the world: An overview with emphasis on the Iberian Peninsula. Pages 1–25 *in* M. B. Morales and J. Traba, editors. Steppe Ecosystems: Biological Diversity, Management and Restoration. NOVA Science Publishers, New York,

USA.

Sainz Ollero, H., and M. A. van Staalduinen. 2012. Iberian Steppes. Pages 273–288 Eurasian steppes: ecological problems and livelihoods in a changing world.

Salamí, E., C. Barrado, and E. Pastor. 2014. UAV flight experiments applied to the remote sensing of vegetated areas. Remote Sensing 6:11051–11081.

Sardà-Palomera, F., G. Bota, C. Viñolo, O. Pallarés, V. Sazatornil, L. Brotons, S. Gomáriz, and F. Sardà. 2012. Fine-scale bird monitoring from light unmanned aircraft systems. Ibis 154:177–183.

Serrano, L., J. A. Gamon, and J. Penuelas. 2000. Estimation of canopy photosynthetic and nonphotosynthetic components from spectral transmittance. Ecology 81:3149–3162.

Siemann, E. 1998. Experimental tests of effects of plant productivity and diversity on grassland arthropod diversity. Ecology 79:2057–2070.

Smith, B. M., N. J. Aebischer, J. Ewald, S. Moreby, C. Potter, and J. M. Holland. 2020. The Potential of Arable Weeds to Reverse Invertebrate Declines and Associated Ecosystem Services in Cereal Crops. Frontiers in Sustainable Food Systems 3:118.

Southwood, T. R. E., V. K. Brown, and P. M. Reader. 1979. The relationships of plant and insect diversities in succession. Biological Journal of the Linnean Society 12:327–348.

Sripada, R. P., R. W. Heiniger, J. G. White, and A. D. Meijer. 2006. Aerial color infrared photography for determining early in-season nitrogen requirements in corn. Agronomy Journal 98:968–977.

Srivastava, D. S., and J. H. Lawton. 1998. Why more productive sites have more species: An experimental test of theory using tree-hole communities. American Naturalist 152:510–529.

Strong, C. J., N. G. Burnside, and D. Llewellyn. 2017. The potential of small-Unmanned Aircraft Systems for the rapid detection of threatened unimproved grassland communities using an Enhanced Normalized Difference Vegetation Index. PLoS ONE 12:e0186193.

Sweet, S. K., A. Asmus, M. E. Rich, J. Wingfield, L. Gough, and N. T. Boelman. 2015. NDVI as a predictor of canopy arthropod biomass in the Alaskan arctic tundra. Ecological Applications 25:779–790.

Thomas, J. A., M. G. Telfer, D. B. Roy, C. D. Preston, J. J. D. Greenwood, J. Asher, R. Fox, R. T. Clarke, and J. H. Lawton. 2004. Comparative Losses of British Butterflies, Birds, and Plants and the Global Extinction Crisis. Science 303:1879–1881.

Traba, J., M. B. Morales, E. L. García De La Morena, M. P. Delgado, and A. Krištín. 2007. Selection of breeding territory by little bustard (Tetrax tetrax) males in Central Spain: The role of arthropod availability. Ecological Research 23:615–622.

Traba, J., P. Sastre, and M. B. Morales. 2013. Factors determining species richness and composition of steppe bird communities in Peninsular Spain: Grass-steppe vs. shrub-steppe bird species. Pages 47–72 *in* M. B. Morales and J. Traba, editors. Steppe Ecosystems: Biological Diversity, Management and Restoration. NOVA Science Publishers, New York, USA.

Upadhyay, P., S. K. Ghosh, and A. Kumar. 2013. High resolution temporal normalized difference vegetation indices for specific crop identification. ISPRS - International Archives of the Photogrammetry, Remote Sensing and Spatial Information Sciences XL-1/W1:351–355.

Vermeulen, C., P. Lejeune, J. Lisein, P. Sawadogo, and P. Bouché. 2013. Unmanned Aerial Survey of Elephants. PLoS ONE 8:e54700.

Viña, A., A. A. Gitelson, A. L. Nguy-Robertson, and Y. Peng. 2011. Comparison of different

vegetation indices for the remote assessment of green leaf area index of crops. Remote Sensing of Environment 115:3468–3478.

Weiss, N., H. Zucchi, and A. Hochkirch. 2013. The effects of grassland management and aspect on Orthoptera diversity and abundance: Site conditions are as important as management. Biodiversity and Conservation 22:2167–2178.

Weyer, J., J. Weinberger, and A. Hochkirch. 2012. Mobility and microhabitat utilization in a flightless wetland grasshopper, Chorthippus montanus (Charpentier, 1825). Journal of Insect Conservation 16:379–390.

Zurdo, J., J. Baonza, and J. Traba. 2021. New insights on plant communities and flora of the southern paramos of the Iberian Range (Spain). Phytocoenologia 50:371–382.

Zuur, A. F., E. N. Ieno, and A. A. Saveliev. 2017. Beginner's guide to spatial, temporal, and spatial-temporal ecological data analysis with R-INLA. Page Highland Statistics Ltd. Newburgh, U.K.

TABLES

Table 1. Number of sampling stations located per month and year in the whole study area (sampling stations) and within UAV flight plots (sampling stations UAV plots). In addition, we indicate whether S2 and UAV imagery were available for each sampling period. Lastly, we indicate within brackets the number of plots where the UAV flights were carried out. Those samplings for which neither S2 nor UAV imagery were available, are omitted.

Season	Month	Sampling stations	Sentinel-2 imagery	Sampling stations UAV plots	UAV flights
2017					
Spring	April	79	Yes	0	No
	June	79	Yes	41	Yes (6)
Summer	July	79	Yes	0	No
Autumn	October	79	Yes	41	Yes (6)
2018					
Spring	April	67	No	48	Yes (7)
	June	67	Yes	48	Yes (7)
Summer	July	67	Yes	0	No
Autumn	October	67	Yes	48	Yes (7)
2019					
Winter	January	67	Yes	0	No
Spring	May	67	Yes	0	No
	June	67	Yes	0	No
Summer	July	67	Yes	0	No
Autumn	September	67	Yes	0	No

Table 2. Formulas used to calculate each vegetation index. NIR refers to the Near-infrared spectral band. The NIR band was used to calculate the vegetation indices from Sentinel-2 imagery, but it was replaced by the Red-edge (RE) spectral band for the vegetation indices calculated from UAV imagery.

	Index	Formula	Reference
NDVI	*Normalized Difference Vegetation Index*	$\frac{\rho_{NIR} - \rho_{Red}}{\rho_{NIR} + \rho_{Red}}$	
BNDVI	*Blue Normalized Difference Vegetation Index*	$\frac{\rho_{NIR} - \rho_{Blue}}{\rho_{NIR} + \rho_{Blue}}$	
ENDVI	*Enhanced Normalized Difference Vegetation Index*	$\frac{(\rho_{NIR} + \rho_{Green}) - (2 * \rho_{Blue})}{(\rho_{NIR} + \rho_{Green}) + (2 * \rho_{Blue})}$	
GIPVI	*Green Infrared Percentage Vegetation Index*	$\frac{\rho_{NIR}}{\rho_{NIR} + \rho_{Green}}$	Crippen, 1990
GNDVI	*Green Normalized Difference Vegetation Index*	$\frac{\rho_{NIR} - \rho_{Green}}{\rho_{NIR} + \rho_{Green}}$	Gitelson et al. 1996
GRVI	*Green Ratio Vegetation Index*	$\frac{\rho_{NIR}}{\rho_{Green}}$	Sripada et al. 2006
GSAVI	*Green Soil Adjusted Vegetation Index*	$\frac{\rho_{NIR} - \rho_{Green}}{(\rho_{NIR} + \rho_{Green} + L)} * (1 + L)$ with L = 0.5	

Table 3. Summary statistics of the vegetation indices calculated from UAV and Sentinel-2 imagery. The mean, the standard deviation (SD), and the range [minimum; maximum] are shown. The NDVI index could not be calculated for the UAV imagery because the sensor employed did not provide images along the Red spectral band. VI names are provided in Table 2.

	UAV			Sentinel-2		
	Mean	**SD**	**Range**	**Mean**	**SD**	**Range**
BNDVI	0.15	0.04	[0.08; 0.24]	0.56	0.04	[0.46; 0.66]
ENDVI	0.07	0.03	[0.02; 0.15]	0.43	0.04	[0.34; 0.53]
GIPVI	0.58	0.01	[0.56; 0.62]	0.71	0.02	[0.67; 0.76]
GNDVI	0.17	0.03	[0.12; 0.24]	0.42	0.03	[0.35; 0.51]
GRVI	1.41	0.08	[1.27; 1.62]	2.49	0.20	[2.07; 3.11]
GSAVI	0.25	0.04	[0.18; 0.35]	0.63	0.05	[0.52; 0.77]
NDVI	-	-	-	0.31	0.05	[0.20; 0.48]

Table 4. Summary statistics of the biomass of epigeous and coprophagous arthropods as well as the four functional consumer groups (predatory, detritivore, phytophagous and diverse). The mean, the standard deviation (SD), and the maximum value are shown.

	Winter			Spring			Summer			Autumn		
	Mean	**SD**	**Max**	**Mean**	**SD**	**Max**	**Mean**	**SD**	**Max**	**Mean**	**SD**	**Max**
Epigeous	24.1	22.6	114.0	503.0	468.0	3783.7	479.6	381.4	2083.1	379.7	415.5	2666.5
Coprophagous	23.2	68.7	526.9	513.6	1397.2	10219.2	846.8	1519.3	10521.8	687.8	1499.3	9980.8
Predatory	17.8	19.2	96.2	103.7	119.0	1158.9	65.3	65.7	488.8	81.0	141.7	1210.5
Detritivore	0.7	2.1	10.7	164.9	280.7	2424.6	105.9	163.9	1098.8	8.3	19.6	131.8
Phytophagous	4.3	7.0	30.5	155.7	190.0	1404.0	233.8	300.0	1879	262.7	374.4	2555.2
Diverse	0.2	0.6	4.5	67.6	225.0	3434.5	69.5	114.6	1072.8	26.6	116.6	1643.8

Table 5. Results of the Gaussian spatial models addressing the relationship between the biomass of epigeous and coprophagous arthropods, and the vegetation indices calculated from UAV imagery. Models were fitted using data from 41 sampling stations in Spring and Autumn 2017, and 48 sampling stations in Spring, Summer, and Autumn 2018. Posterior mean (β), standard deviation (SD) and 95% Bayesian Credible interval (95% BCI) are shown for each vegetation index, and both epigeous and coprophagous biomass.

	Term	**β**	**SD**	**95% BCI**
Epigeous				
BNDVI	Linear	0.345	0.042	[0.261; 0.427]
ENDVI	Linear	0.319	0.043	[0.234; 0.403]
GIPVI	Linear	0.290	0.046	[0.198; 0.381]
GNDVI	Linear	0.290	0.046	[0.198; 0.381]
GRVI	Linear	0.305	0.047	[0.213; 0.397]
GSAVI	Linear	0.289	0.046	[0.198; 0.381]
Coprophagous				
BNDVI	Linear	0.485	0.079	[0.331; 0.639]
ENDVI	Linear	0.503	0.075	[0.355; 0.651]
GIPVI	Linear	0.404	0.089	[0.229; 0.580]
GNDVI	Linear	0.404	0.089	[0.230; 0.578]
GRVI	Linear	0.402	0.090	[0.226; 0.578]
GSAVI	Linear	0.404	0.089	[0.230; 0.579]

Table 6. Results of the Gaussian spatial models addressing the relationship between the biomass of epigeous and coprophagous arthropods, and the vegetation indices calculated from Sentinel-2 imagery. Models were fitted using data from 79 sampling stations in Spring, Summer and Autumn 2017, and 67 sampling stations in Spring, Summer, and Autumn 2018 and 2019, and Winter 2019. Posterior mean (β), standard deviation (SD) and 95% Bayesian Credible interval (95% BCI) are shown for each vegetation index, and both epigeous and coprophagous biomass.

	Term	**β**	**SD**	**95% BCI**
Epigeous				
BNDVI	Linear	0.029	0.015	[0.001; 0.058]
	Quadratic	0.033	0.013	[0.007; 0.059]
ENDVI	Linear	0.037	0.014	[0.008; 0.065]
	Quadratic	0.034	0.013	[0.008; 0.060]
GIPVI	Linear	-0.006	0.043	[-0.091; 0.079]
GNDVI	Linear	-0.006	0.043	[-0.091; 0.079]
GRVI	Linear	0.005	0.039	[-0.071; 0.082]
GSAVI	Linear	-0.006	0.043	[-0.091; 0.079]
NDVI	Linear	-0.130	0.041	[-0.211; -0.049]
Coprophagous				
BNDVI	Linear	0.439	0.115	[0.213; 0.664]
ENDVI	Linear	0.441	0.105	[0.234; 0.648]
GIPVI	Linear	0.261	0.118	[0.030; 0.492]
GNDVI	Linear	0.261	0.118	[0.030; 0.492]
GRVI	Linear	0.211	0.107	[0.001; 0.422]
GSAVI	Linear	0.261	0.118	[0.030; 0.492]
NDVI	Linear	-0.091	0.111	[-0.309; 0.126]

FIGURES

Figure 1. (A) Location of the study area in Soria province, central Spain (black rectangle). (B) Zoom to the study area in southern Soria. Sampling stations (white dots) and UAV plots (red limits) are depicted. The name of the Special Areas of Conservation (SAC) and Special Protection Areas (SPA) for birds of the European Union's Natura 2000 Network (ES4170148 and ES4170120, respectively) are indicated in bold, and their limits are indicated (black line). (C) Zoom to two UAV plots (black rectangle in panel B), with sampling stations (white dots). The limit of the "Altos de Barahona" SPA is depicted with dashed grey line.

Figure 2. Relationship between the biomass of epigeous arthropods and the vegetation indices calculated from UAV imagery. The mean (black line) and 95% BCI (grey surface) of the values predicted by the models, are depicted. Moreover, the observation values for each sampling station (points) are shown.

Figure 3. Relationship between the biomass of coprophagous arthropods and the vegetation indices calculated from UAV imagery. The mean (black line) and 95% BCI (grey surface) of the values predicted by the models, are depicted. Moreover, the observation values for each sampling station (points) are shown.

Figure 4. Relationship between the biomass of epigeous arthropods and the vegetation indices calculated from Sentinel-2 imagery. The mean (black line) and 95% BCI (grey surface) of the values predicted by the models, are depicted. Moreover, the observation values for each sampling station (points) are shown.

Figure 5. Relationship between the biomass of coprophagous arthropods and the vegetation indices calculated from Sentinel-2 imagery. The mean (black line) and 95% BCI (grey surface) of

the values predicted by the models, are depicted. Moreover, the observation values for each sampling station (points) are shown.

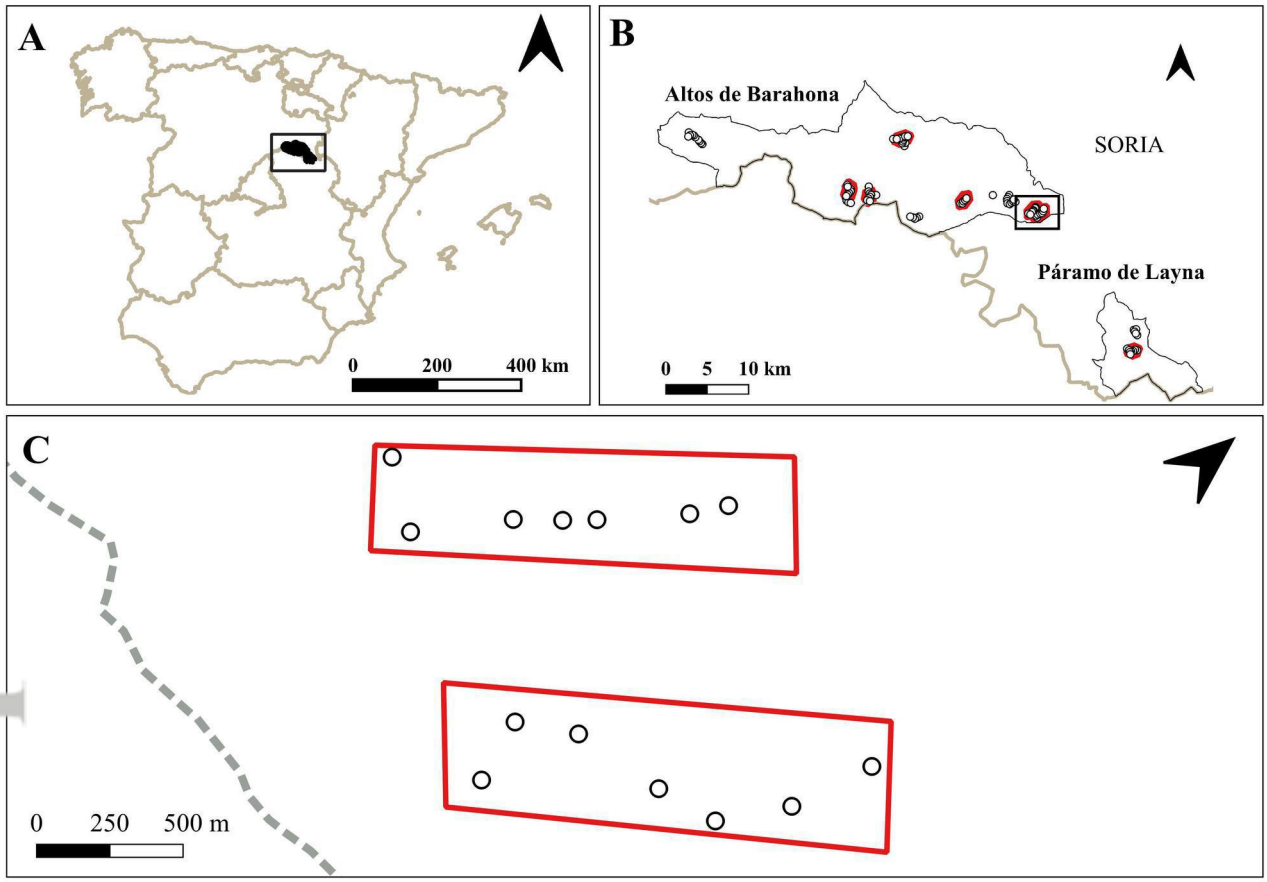

EAP_2707_Figure1.jpeg

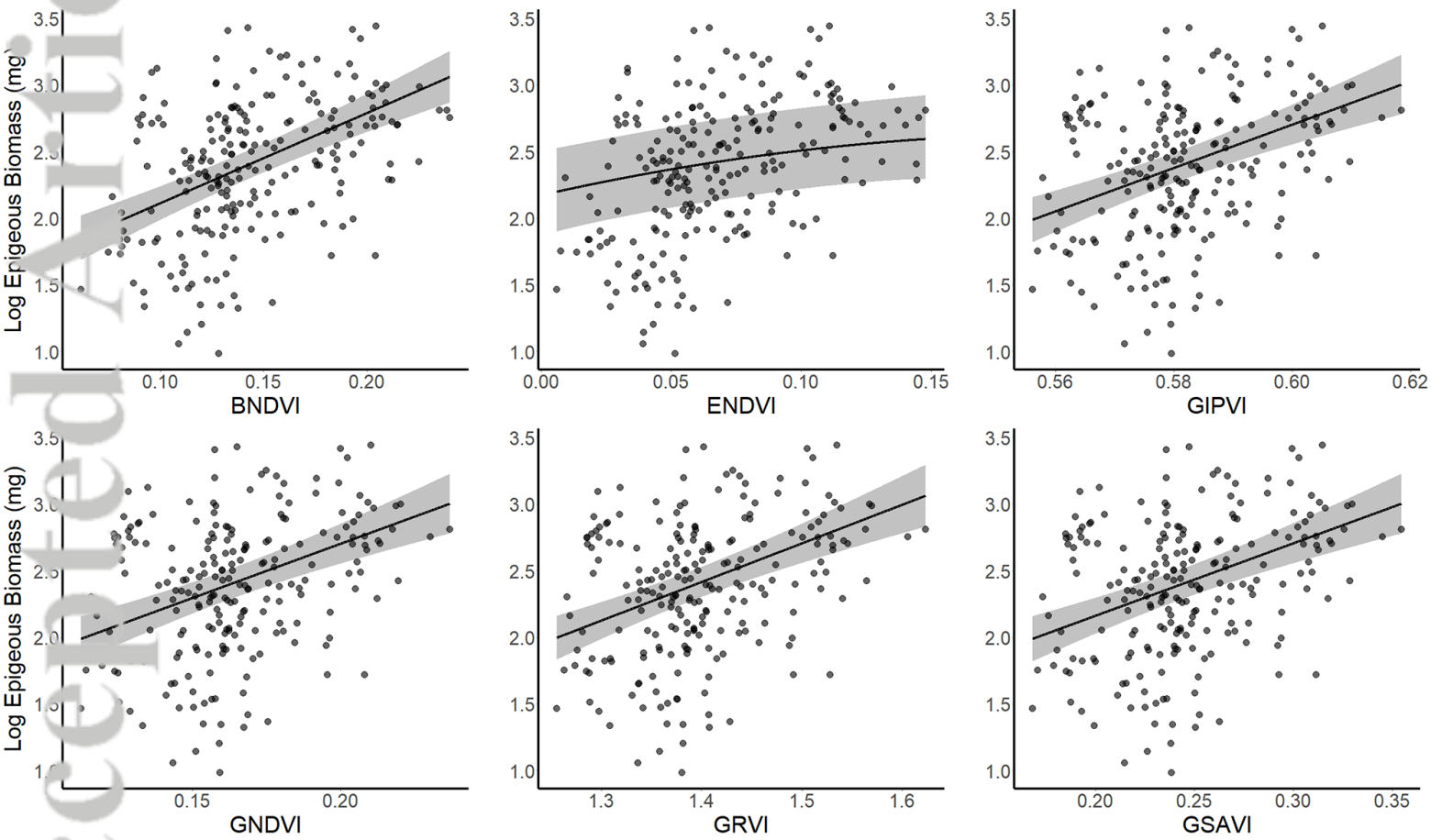

EAP_2707_Figure2.png

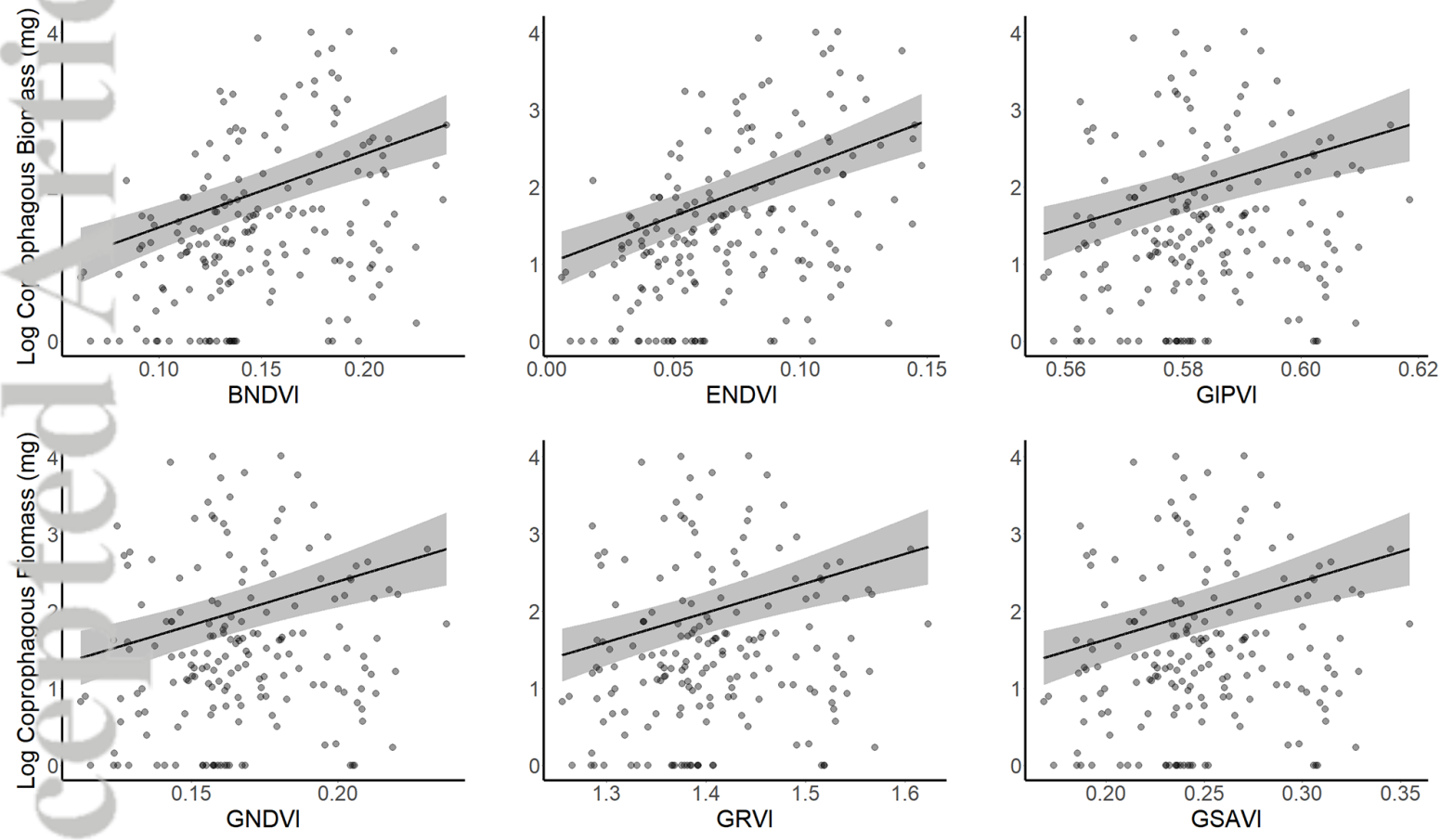

EAP_2707_Figure3.png

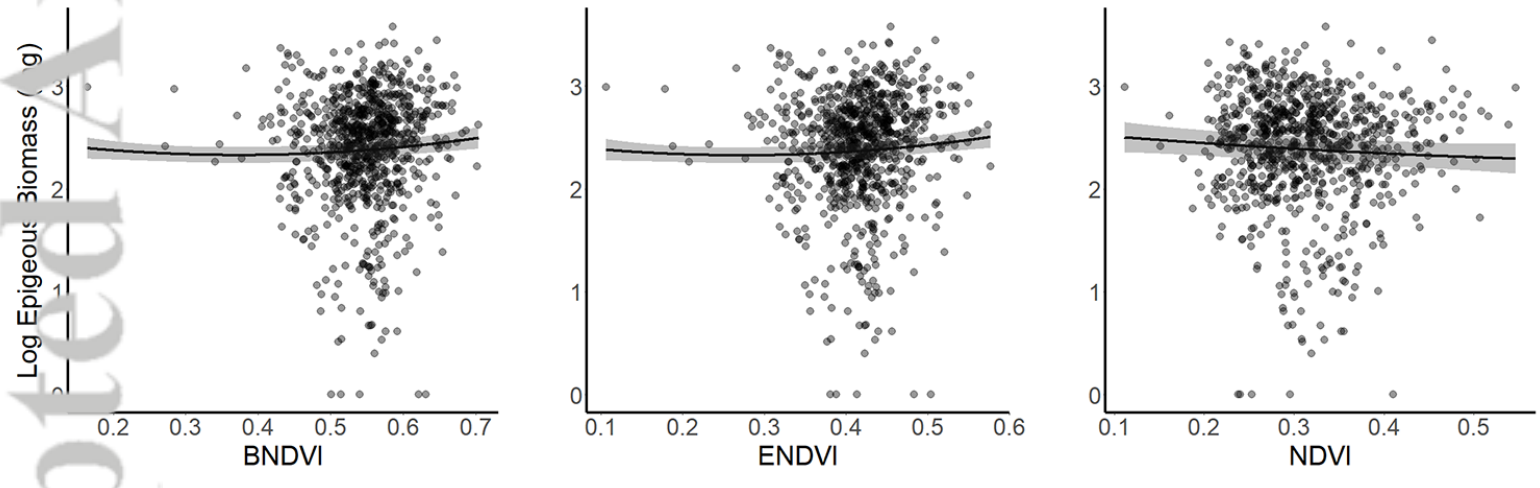

EAP_2707_Figure4.png

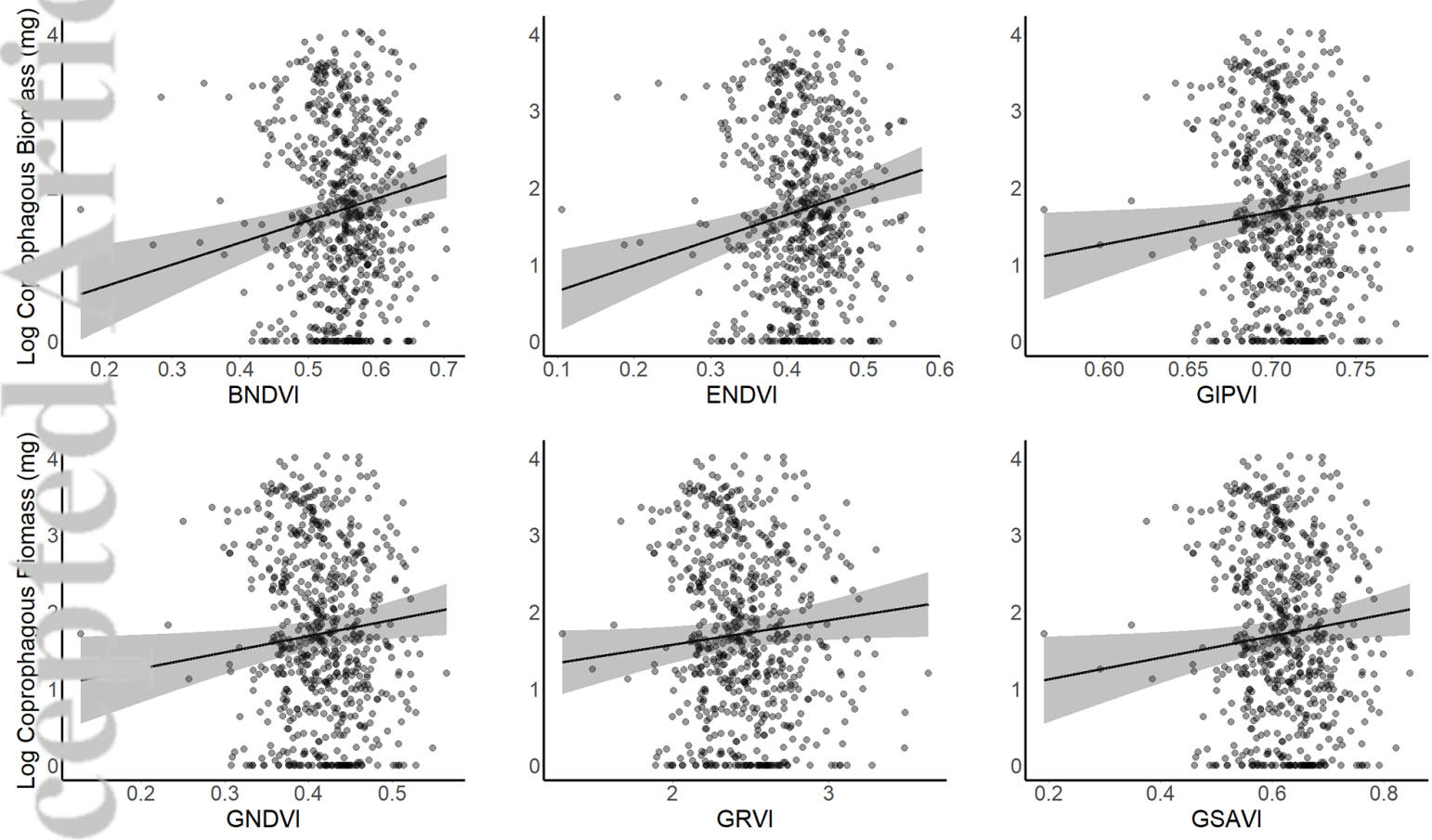

EAP_2707_Figure5.png